Shear band propagation in trapdoor experiments from discrete element and centrifuge modelling

C. Purchase[1,2], S.W. Jacobsz[1] & N.D. Wilke[1]
1. University of Pretoria, Pretoria, South Africa
2. Jones & Wagener (Pty) Ltd, Johannesburg, South Africa

ABSTRACT: Sinkholes are a common occurrence in Centurion, South Africa. The mechanisms associated with the propagation of a subsurface cavity to the soil surface during the formation of a sinkhole are poorly understood, resulting in overly conservative and potentially unrealistic methods for assessing the size of sinkholes. A series of deep-seated trapdoor experiments, using natural granular materials as well as glass beads, were conducted in a centrifuge facility. Strain paths and displacement contours associated with the glass beads centrifuge test, obtained by means of Particle Image Velocimetry (PIV), were used to calibrate corresponding trapdoor experiments using the Discrete Element Method (DEM). Several DEM experiments were then analysed to determine the effect of the overburden material shear strength on shear band propagation associated with sinkhole development. The results of both centrifuge and DEM experiments demonstrated that increased particle interlock, related to greater soil shear strength, resulted in near vertical propagation of the shear bands to the surface. A lower shear strength, resulting from more rounded particles, resulted in a wider overburden failure zone.

1 INTRODUCTION

South Africa's Gauteng Province is not only the smallest province, but also the greatest contributor to the country's GDP. As approximately 25 % of the province is underlain by dolomite, an astute understanding of the mechanisms associated with sinkhole propagation dolomitic soils is essential to ensure the optimal utilisation of land.

The current standard for developing infrastructure on dolomitic land, SANS-1936 (2012), recommends using the method of scenario supposition, developed by Buttrick & Van Schalkwyk (1995), to determine the maximum potential size of a sinkhole. As illustrated in Figure 1, the maximum surface diameter of a sinkhole is highly dependent on both the depth of the subsurface cavity and the selected angle of draw assigned to each of the blanket materials (layers) through which the sinkhole propagates. This method is, however, known to predict very conservative (large) sinkhole sizes (Jacobsz 2016).

Sinkhole formation in South African dolomitic soils is typified by the collapse of a stable arch, spanning the throat of an underlying cavity (Fig. 1) in dolomitic residuum overburden material. The spanning mechanism, often referred to as arching, is associated with the redistribution of stresses within the overburden material, as load is transferred to the abutments of the arch with a loss of subsurface support. A disturbing agent is required to alter the equilibrium of the stable arch causing the arch to migrate to the surface in an "onion-peeling" manner (Jennings et al. 1965).

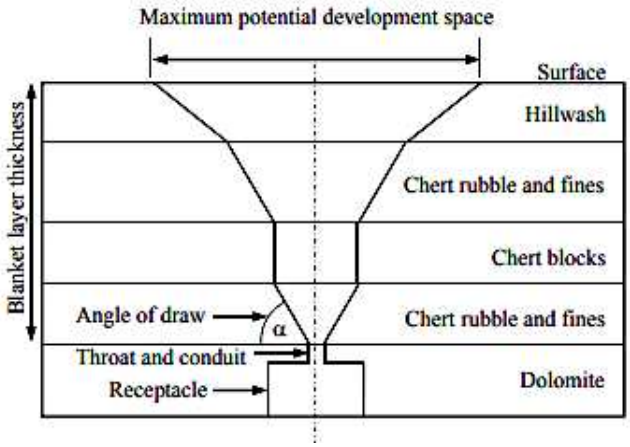

Figure 1. Estimation of the maximum potential development space of a sinkhole (modified from Buttrick & Van Schalkwyk, 1995).

Terzaghi (1936) was the first to investigate the arching effect by means of a trapdoor experiment. The trapdoor experiment consists of a confined mass of geomaterial underlain by a vertically translating trapdoor. The downward displacement of the trapdoor simulates the loss of subsurface support and associated redistribution of stresses, or arching, of the material directly above the trapdoor. It was on this basis

that the trapdoor experiment was selected to be used to investigate the propagation of shear bands, associated with the loss of subsurface support during sinkhole cavity propagation.

As granular materials are inherently discontinuous, the discrete nature of the DEM is suited to study the flow of granular material and it is considered the ideal tool for the investigation of large soil deformations in which the propagation of material discontinuities governs soil behaviour. In the past, work related to DEM simulations of granular material had been restricted due to the limited computing capabilities of conventional CPU-based DEM codes. BlazeDEM, a GPU-based DEM program, developed at the University of Pretoria (Govender 2015), was used in this study, thereby overcoming particle scaling limitations due to its enhanced computing ability.

A set of conventional trapdoor experiments were undertaken in the centrifuge at the University of Pretoria to simulate typical field stress conditions associated with sinkhole formation in dolomitic ground. Trapdoor experiments, using different silica sands as well as glass beads, were conducted to investigate the effect of material shear strength on the failure mechanisms associated with sinkhole propagation. The results of the glass bead trapdoor experiment were used to calibrate the DEM numerical model. Once calibrated, a series of DEM trapdoor experiments were conducted in which a range of inter-particle rolling and sliding friction coefficients were imposed to investigate the deformation patterns associated with materials of various shear strengths.

The purpose of this study was to ascertain the effect of a variation in material shear strength on the mechanisms associated with cavity propagation during sinkhole formation.

2 CENTRIFUGE TRAPDOOR EXPERIMENTS

2.1 *Centrifuge model*

The strongbox in which the material was housed during testing consisted of a 10 mm aluminium back plate, two aluminium channel profiles forming the side walls and a 20 mm thick tempered glass window which acted as the front face of the strongbox. The glass window pane facilitated the observation of the cavity propagation in two-dimensional plane-strain conditions during trapdoor displacement. A schematic of the strongbox is presented in Figure 2. As illustrated, a translating trapdoor with a width of 50 mm, was located in the centre of the strongbox base.

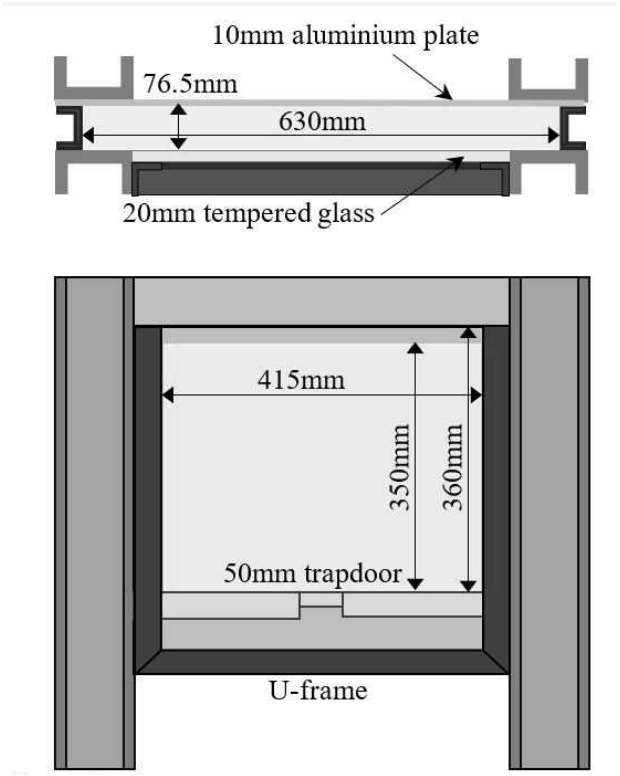

Figure 2. Schematic of the strongbox and trapdoor apparatus used in the centrifuge trapdoor experiments

The trapdoor was set to displace continuously at a rate of 0.025 mm/s. The trapdoor translation was controlled by means of a hydraulic system in which a linear actuator with a stepper motor, connected to a water-filled cylinder, was used to extract water from another cylinder supporting the trapdoor. A centripetal acceleration of 50 g was applied in the centrifuge, so that the trapdoor width corresponded to a sinkhole diameter of 2.5 m and an approximate vertical stress of 300 kPa at the base of the strongbox (material dependent).

The centrifuge models were prepared by means of pluviation using an overhead sand hopper. A consistent drop height and a comparatively slow and uniform flow rate resulted in dense and uniform bulk material packings.

2.2 *Materials tested*

The centrifuge trapdoor experiments were conducted using fine-grained silica sand, coarse-grained silica sand and 2 mm glass beads. The coarse sand comprised of rounded grains, whereas the fine sand was sub-angular. Both materials were sourced commercially.

The particle size distributions of the materials are presented in Figure 3. Three very dense material models were prepared, i.e. with relative densities exceeding 90 %. The significant material properties are summarised in Table 1.

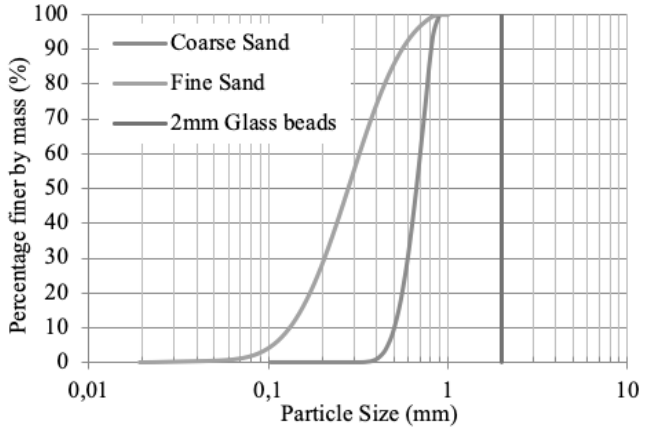

Figure 3. Particle size distribution of the geomaterials used in the centrifuge trapdoor experiments

Table 1. Centrifuge experiment material properties

	Materials		
	Coarse Sand*	Fine Sand	Glass beads
D_{50} (mm)	0.737	0.307	2.0
φ'_{peak} (°)	39.0	42.3	16.8
$\varphi'_{critical\ state}$ (°)	32.0	34.8	15.7
G_s (g/cm^3)	2.654	2.675	2.5
$\rho_{d\ max}$ (kg/m^3)	1773	1590	1603#
$\rho_{d\ min}$ (kg/m^3)	1709	1502	1400#

* Coarse sand material properties from Archer (2014)
\# Random packing arrangement of uniform spheres

3 RESULTS OF CENTRIFUGE EXPERIMENTS

GeoPIV (Stanier et al. 2015) was used to produce maximum shear strain plots from the photographic record of the centrifuge tests. Inflight photographs and corresponding shear strain surface plots of the fine-grained Afrimat sand at 5 mm, 40 mm and 80 mm trapdoor displacement are presented in Figure 4.

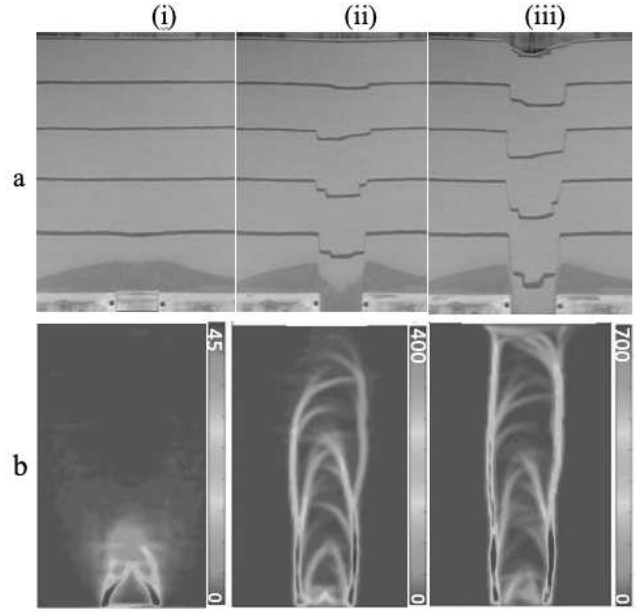

Figure 4. The (a) inflight photographs and (b) maximum shear strain plots for the fine-grained sand at (i) 5 mm, (ii) 40 mm and (iii) 80 mm trapdoor displacement (units in percentage)

At the onset of the trapdoor displacement, the dilation of both granular materials was evident as shear bands propagated from the edges of the trapdoor to form triangular arrangements of shear bands. The stable triangular wedge of granular material then translated downwards, with the trapdoor, until an additional shear band propagated from one or both of the trapdoor edges at a lesser angle to the vertical. With further lowering of the trapdoor the propagation of new shear bands for both the fine- and coarse-grained sands become non-symmetric, appearing to alternate from either side of the trapdoor, propagating in an upward direction (Fig. 4b(ii)) until the two vertical shear bands reached the surface. The column of material between the two vertical shear bands then simply displaced downwards with further trapdoor translation.

With an increase in trapdoor displacement, the shear bands associated with the glass beads trapdoor experiment propagate away from the trapdoor centreline to form an inverted triangular mechanism before narrowing towards the surface, forming an approximately ellipse-shaped (ellipsoidal) deformation pattern at relatively large trapdoor displacements. Maximum shear strain distributions of the three tests, at 80 mm trapdoor displacement, are displayed in Figure 5.

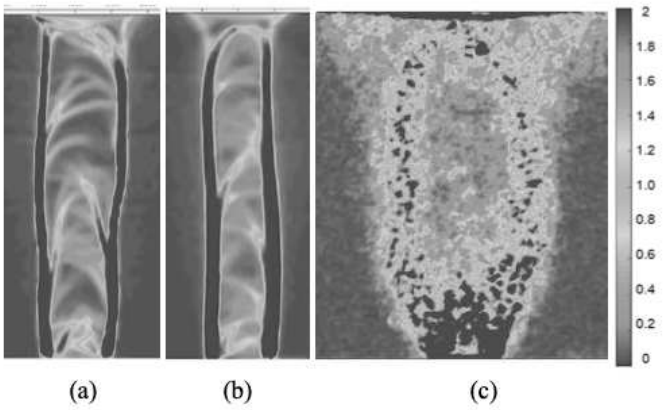

Figure 5. Maximum total shear strain plots at 80 mm trapdoor displacement: (a) Fine Sand, (b) Coarse Sand and (c) Glass beads (unitless)

These deformation patterns indicate that a significantly greater zone of material is influenced in the glass beads model in comparison to that of the granular materials at the same trapdoor displacement. The wider zone of influence is attributed to the comparatively lower shear strength of the material.

It is well-known that the shear band width is a function of the average particle size. The shear band widths for fine-grained sand, coarse-grained sand and glass beads in Figure 5a, b and c, respectively, demonstrate a distinct increase in the width of the shear bands with increasing particle size.

Vertical displacement contours and maximum shear strain plots of the glass bead centrifuge test were used to calibrate the corresponding DEM model with spherical particles.

4 DEM TRAPDOOR EXPERIMENT MODEL

4.1 *Overview of DEM*

The Discrete Element Method, pioneered by Cundall & Strack (1979), is an explicit numerical modelling method in which soil grains are idealised as individual particles. The primary purpose of this numerical method is to describe the global behaviour of an assembly of individual particles to a disturbance of the material. Simply put, DEM is founded on a force-displacement law for the normal (Eq. 1) and tangential (Eq. 2) directions, as well as Newton's second law of motion for translation (Eq. 3) and rotation (Eq. 4):

$$F_n = -k_n.\Delta n_n + c_n.v_n \quad (1)$$

where F_n = normal contact force; k_n = normal contact stiffness; Δn_n = normal inter-particle overlap; c_n = normal damping coefficient; and v_n = normal inter-particle relative velocity. The tangential force on a particle is calculated incrementally as detailed below, with the maximum tangential contact force dictated by the coefficient of friction (μ) according to $F_t \leq \mu F_n$:

$$F_t = \int_{t_0}^{t} k_t\,\Delta v_t.dt + c_t.\Delta v_t \quad (2)$$

where F_t = tangential (shear) contact force; k_t = tangential contact stiffness; v_t = tangential inter-particle relative velocity; and c_t = tangential damping coefficient (Wang, 2017). Newton's second law of motion for translation is as follows:

$$m_i \frac{d^2}{dt^2}\vec{x_i} = m_i\vec{g} + \sum_{N_c}\left(\vec{f_{nc}} + \vec{f_{tc}}\right) \quad (3)$$

where m_i = mass of particle i; x_i = position of particle i centroid; g = gravitational acceleration; f_{nc} = sum of normal inter-particle contact forces; and f_{tc} = sum of tangential inter-particle contact forces. Finally, the rotation of a particle is governed by Newton's second law of rotation:

$$I_i \frac{d}{dt}\vec{\omega_i} = \sum_{Nc}\vec{r_c} \times \vec{f_{tc}} + \vec{M_r} \quad (4)$$

where I_i = moment of inertia about grain centroid; ω_i = angular velocity of particle i; r_c = vector from particle mass centre to contact point; and M_r = rolling resistant moment (Zhao 2017).

The basic contact model utilised in the DEM numerical experiments was the linear spring-dashpot model, shown in Figure 6. The fundamental particle parameters are as follows:

- The particle contact spring stiffnesses (k_n and k_t): used to simulate the elastic contact force between two particles during a collision (spring)
- Damping coefficients (c_n and c_t): used to simulate energy dissipation during a collision (dashpot). These are a function of the material's coefficient of restitution (CoR).
- Friction coefficient (μ): used to apply a resistance to particle-particle sliding (slider)
- Rolling friction coefficient (μ_r): used to apply a resistance to particle rotation. This parameter dictates the maximum applied rolling moment according to Eq. 5 (not included in Figure 6):

$$M_p = \mu_r.r.|F_n| \quad (5)$$

where M_p = maximum rolling moment; and r = average particle radius.

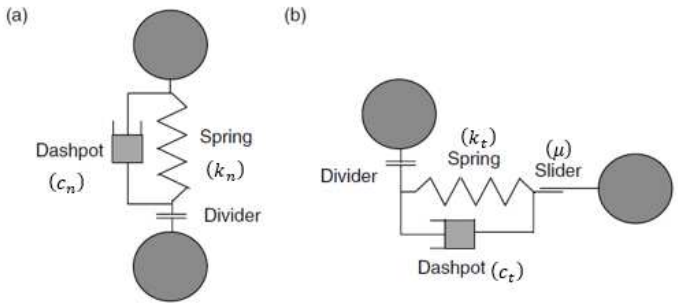

Figure 6. Linear spring-dashpot contact models for the (a) normal and (b) tangential directions (from Jiang, et al., 2006)

An important assumption in the DEM formulation is that particle velocity and acceleration remain constant within a single timestep. The time step refers to the time increment between each iteration of the calculation cycle in which the dynamic equilibrium of the individual particles is maintained. O'Sullivan (2011) highlights the importance of limiting the duration of the time step to ensure numerical stability of the system. The smaller the time step, the greater the computational cost of the simulation.

The particle normal stiffness is directly proportional to both the particle radius and material's Young's Modulus (E). Contrarily, the required time step is inversely proportional to the Young's Modulus of the material (Thakur et al. 2016). Therefore, the higher the particle normal stiffness, the smaller the required time-step and the greater the computational effort required to run the analysis. It is therefore common practice to reduce the particle normal stiffness to reduce load (Yousefi & Ng 2017).

Continuum-based numerical models, such as the Finite Element or Finite Difference Methods (FEM or FDM, respectively), are often used to investigate the behaviour of geomaterials. These methods assign a constitutive law to the soil continuum to describe its stress-strain response to an external force or disturbance. Over and above the fact that a suitable stress-strain constitutive law for continuum modelling may not exist, the description of a discontinuity or localisation in a soil continuum is a complex problem, specifically when granular flow or the propagation of numerous cracks are simulated (O'Sullivan 2011). DEM overcomes these primary shortcomings as the particle boundaries in the DEM model represent the physical discontinuities in a granular medium. A complex constitutive model is therefore not required. However, a

significant disadvantage of DEM is that it is computationally expensive to simulate granular problems, particularly at large scales.

4.2 *Significance of GPU-based DEM codes*

One of the latest developments in DEM numerical modelling is the utilisation of Graphical Processing Units (GPUs) instead of more conventional Central Processing Units (CPUs). GPUs are able to process a large number of simple arithmetic operations in parallel whereas CPUs are better suited to solving complex individual problems. A decoupled algorithm in which the fundamental DEM calculation cycle is processed is therefore required to optimise the utilisation of the GPU framework (Govender et al. 2016).

Blaze-DEM, the DEM code used in this study, is a three-dimensional high-performance research code that was developed by Govender (2015) at the University of Pretoria and CSIR. The Blaze-DEM framework was developed for GPU architecture and therefore utilises the parallelism of a GPU cluster.

4.3 *Blaze-DEM trapdoor experiments*

The width and depth of the numerical model was reduced relative to the physical model to 325 mm and 18.2 mm, respectively, while the height of the model remained unchanged at 360 mm.

The numerical trapdoor experiment was executed in three stages. Initially, the strongbox was filled with 300 000 spherical particles by means of pluviation under normal gravitational conditions. Centrifuge "spin-up" was then simulated by increasing the gravitational acceleration applied to the model to 50 g. Finally, trapdoor displacement was initiated, and the trapdoor continuously lowered at a calibrated rate of 0.02 m/s.

A greater trapdoor displacement rate (0.02 m/s at prototype dimensions in Blaze-DEM, in comparison to 0.025 mm/s at model dimensions in the centrifuge) was applied to reduce the computational effort required to duplicate the centrifuge trapdoor experiment numerically. The particle parameters of the DEM model were calibrated to yield vertical displacement contours analogous to those of the centrifuge experiment at 10 mm trapdoor displacement.

In order to generate shear strain plots of the DEM trapdoor experiments, Delaunay triangulation was applied to the particle centroids of the DEM simulations to create a network of Constant Strain Triangle (CST) elements. The strain formulation by White & Bolton (2004) was then applied to these elements to calculate the associated maximum shear strains. Once the particle parameters had been calibrated satisfactorily for the purposes of this study, the effect of (simulated) particle interlock on the maximum shear strain plots was investigated.

Particle rolling and sliding friction coefficients were increased incrementally in experiments RF1, RF2 and RF3 to simulate varying degrees of particle interlock and its effect on the failure mechanisms of a soil mass subjected to subsurface loss of support.

The calibrated particle parameters, as well as the particle parameters used to investigate the effect of particle interlock on shear band propagation, are summarised in Table 2. The tangential contact stiffness is defined within Blaze-DEM as half of the normal contact stiffness corresponding normal parameters and are thus not listed below. Furthermore, both damping coefficients are calculated within the code and are a function of the input coefficient of restitution (CoR). The CoR was therefore the calibrated parameter as shown in Table 2. It should be noted that two sliding friction coefficients are implemented in Blaze-DEM, namely the static (μ_s) and kinetic (μ_k) friction coefficients. For the purpose of the numerical experiments, the static friction coefficient was kept constant at the calibrated value of 0.18.

Table 2. Calibrated vs trial particle properties for DEM trapdoor experiments

	DEM Experiments			
	Calibrated	RF1	RF2	RF3
CoR	0.9	0.9	0.9	0.9
k_n (N/m)	4.5E+10	4.5E+10	4.5E+10	4.5E+10
k_t (N/m)	2.25E+10	2.25E+10	2.25E+10	2.25E+10
μ_k	0.18	0.2	0.5	0.5
μ_r	0.001	0.2	0.2	0.4

5 RESULTS OF DEM EXPERIMENTS

Maximum shear strain plots from the calibrated numerical model and the trapdoor experiments RF1, RF2 and RF3 were evaluated at a final trapdoor displacement of 80 mm to determine the effect of material shear strength (creating particle interlock) on shear band propagation to the surface of the overburden material. The results of the numerical trapdoor experiments are presented in Figure 7.

In all four models two primary shear bands propagated from the edges of the trapdoor to meet at the surface. Two additional bands then branch off from the primary shearing arms near the top of the soil profile and extend outwards, towards the soil surface. The maximum shear strain plots demonstrate a greater tendency of the shear bands towards verticality with an increase in rolling and sliding friction coefficients. The zone of influence, both in the overburden material and along the soil surface, also narrows with an increase in simulated material shear strength. This observation is made evident by the incremental increase in shear strain magnitude and concentration from Figure 7a to d.

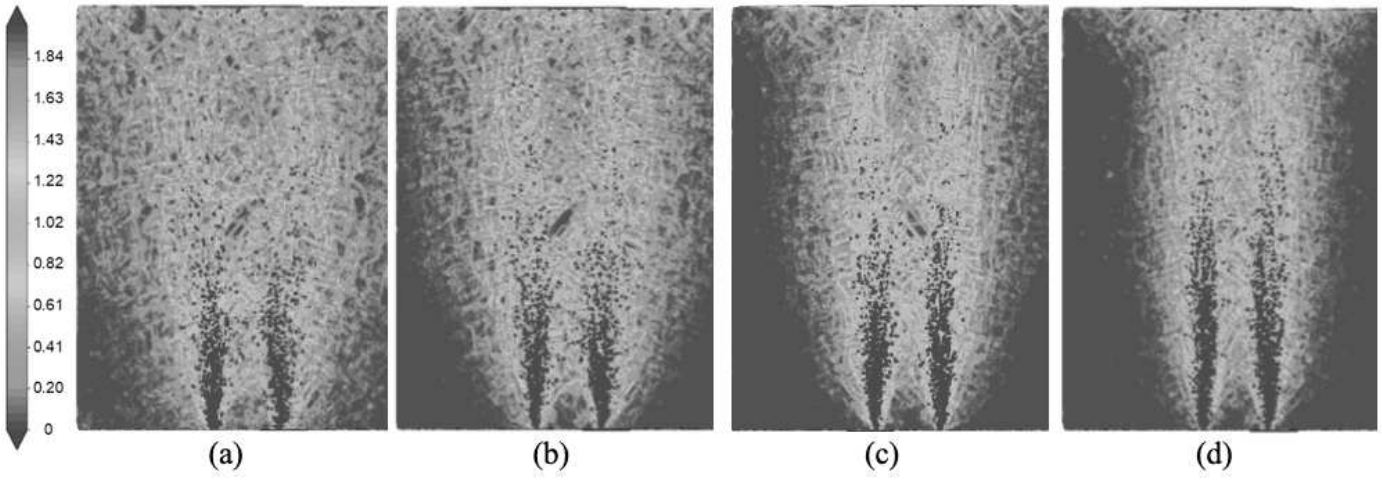

Figure 7. Maximum shear strain surface plots at 80 mm trapdoor displacement for (a) calibrated model, (b) RF1, (c) RF2, and (d) RF3 (unitless)

6 DISCUSSION OF RESULTS

6.1 *Material shear strength*

Based on the shear strain results of the physical trapdoor experiments discussed in Section 3, as well as the results presented in **Error! Reference source not found.**, the width of the ellipsoid or column of material representing the area of soil deformation, and corresponding zone of influence, is governed by the shear strength of the soil. The shear bands of a material with a low shear strength are curved, with the associated deformation ellipsoid tending towards a circular shape. Conversely, a material with a high shear strength generally exhibits a columnar or rectangular deformation shape.

7 CONCLUSIONS

A series of physical and numerical trapdoor experiments were undertaken to investigate the effect of material shear strength on the deformation mechanisms in geomaterials during a loss of subsurface support.

In the physical experiments the granular materials with a greater shear strength yielded vertical shear bands. In contrast, the shear bands in the glass beads model were curved with a significantly wider zone of influence in both the overburden material, as well as at the surface. This trend was confirmed by the numerical trapdoor experiments, as the zone of influence reduced and tended towards verticality with an increase in the assigned magnitude of the friction coefficients.

8 REFERENCES

Archer, A. 2014. *Using small-strain stiffness to predict the settlement of shallow foundations on sand*. MEng dissertation. University of Pretoria.

Buttrick, D. & Van Schalkwyk, A. 1995. The method of scenario supposition for stability evaluation of sites on dolomitic land in South Africa. *Journal of the South African Institution of Civil Engineering.* Fourth quarter 1995: 9-14.

Cundall, P.A. & Strack, O.D. 1979. A discrete numerical model for granular assemblies. *Geotechnique*. 29(1): 47-65.

Govender, N. Wilke, D.N. & Kok, S. 2016. Blaze-DEMGPU: Modular high-performance DEM framework for the GPU architecture. *SoftwareX*. 5: 62-66.

Govender, N. 2015. Blaze-DEM: *A GPU based large scale 3D discrete element particle transport framework.* Doctoral dissertation, University of Pretoria.

Jacobsz, S.W. 2016. Trapdoor experiments studying cavity propagation. *In Proceedings of the first Southern African Geotechnical Conference:* 159-165.

Jennings, J. E. Brink, A.B.A. Louw, A. & Gowan, G.D. 1965. Sinkholes and subsidence in the Transvaal dolomites of South Africa. *Proc 6th International Conference on Soil Mechanics*. Montreal, Canada: 51-54.

Jiang, M.J. Yu, H.S. & Harris, D. 2006. Bond rolling resistance and its effect on yielding of bonded granulates by DEM analyses. *International Journal for Numerical and Analytical Methods in Geomechanics*. 30(8): 723-761.

O'Sullivan, C. 2011. Particle-based discrete element modeling: geomechanics perspective. *International Journal of Geomechanics*. 11(6): 449-464.

South African Bureau of Standards. 2012. *Development of dolomite land - Part 2: Geotechnical investigations and determinations.* SANS 1936-2.

Stanier, S.A. Blaber, J. Take, W.A. & White, D.J. 2015. Improved image-based deformation measurement for geotechnical applications. *Canadian Geotechnical Journal*. 53(5): 727-739.

Terzaghi, K. 1936. Stress distribution in dry and saturated sand above a yielding trap-door. *Proc 1st International Conference of Soil Mechanics*, Harvard University, Cambridge (USA). 1: 307-311.

Thakur, S.C. Ooi, J.Y. & Ahmadian, H. 2016. Scaling of discrete element model parameters for cohesionless and cohesive solid. *Powder Technology*. 293: 130-137.

Wang, J.P. 2017. Force transmission modes of non-cohesive and cohesive materials at the critical state. *Materials*. 10(9): 1014

White, D.J. & Bolton, M.D. 2004. Displacement and strain paths during plane-strain model pile installation in sand. *Géotechnique*. 54(6): 375-397.

Yousefi, A. & Ng, T.T. 2017. Dimensionless input parameters in discrete element modeling and assessment of scaling techniques. *Computers and Geotechnics*. 88: 164-173.

Zhao, T. 2017. *Coupled DEM-CFD analyses of landslide-induced debris flows*. Springer: Singapore.